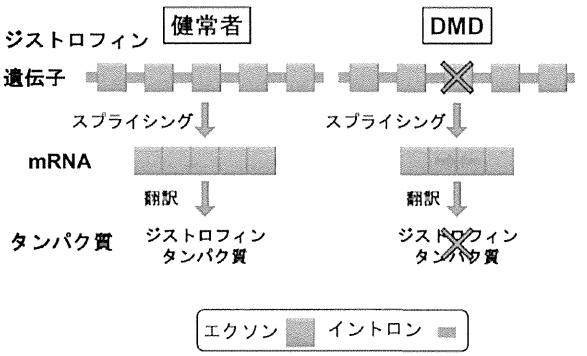

図 1　ジストロフィンタンパク質の合成過程

近年，DMD 患者の壊れかけた筋肉では，炎症やアレルギーなどに関与するプロスタグランジン D_2 合成酵素（PGD_2 synthase : PGDS）の発現が亢進していることが明らかとなった。したがって、DMD の病状診断に PGD_2 の尿中代謝物である tetranor-PGDM（PGDM）濃度の定量が有効であるとの考えに至った。

図 2 に PGD_2 および PGE_2 の生合成・代謝経路を示す。

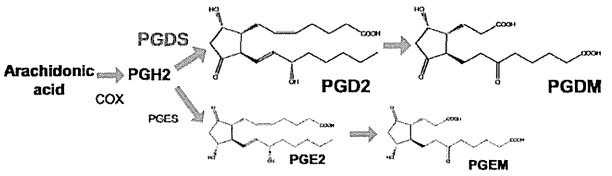

図 2　PGD_2 および PGE_2 の生合成・代謝経路

現在のところ PGDM の測定には、液体クロマトグラフィーと接続した liquid chromatography(LC) -tandem mass spectrometry（LC-MS/MS）法が最も適している。MS（mass spectrometry）は、まず化合物を適切な方法でイオン化し、生成したイオンを *m/z* で分離して、各々の *m/z* のイオン量を測定することで定性・定量分析を行う分析法である。本法は感度がよいことから、ng あるいはそれ以下程度の極微量試料に対して大いに威力を発揮する。本実験では、数ある質量分析法のイオン化、質量分析部の中から、イオン化法としてエレクトロスプレーイオン化（electrospray ionization : ESI）を、質量分析部として四重極質量分析を用いた。ESI は、イオンを溶液から気相へ移すソフトなイオン化法であり、比較的大きな分子量をもち、PGDM のイオン化には適している。tandem mass spectrometry（MS/MS）は、第 1 段階（MS1）において質量選択されたプリカーサーイオンが、活性化された中性種との衝突により衝突誘起解離（CID）を起こし、生じたプロダクトイオンが第 2 段階（MS2）で選択されることで観測する手法である。この測定モードが selected reaction monitoring（SRM）であり、LC-MS/MS は 2 段階の MS 分析すなわち SRM を行うことで、高感度かつ高い選択性で化合物の測定を行うことが可能となる。

また、PGDM は negative ion モードでのイオン化効率が高い。したがって PGDM（MW: 328）は、MS1 でプリカーサーイオン $[M-H]^-$ の *m/z* 327.1、MS2 でプロダクトイオンの *m/z* 143.1 によって定量することにした。内標準として、PGDM-d6 を用いたので、プリカーサーイオン $[M-H]^-$ は *m/z* 333.2、MS2 でプロダクトイオンは *m/z* 149.2 となる（図 3）。

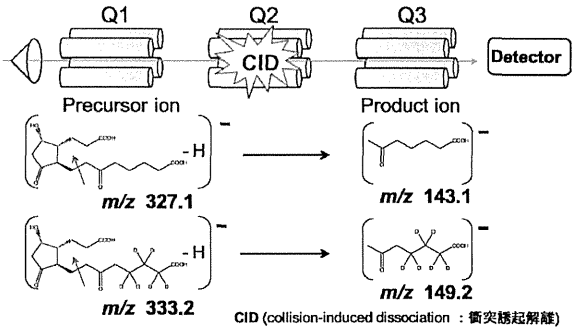

図 3　PGDM の Selected reaction monitoring (SRM)法

24～25 年度は、本法を用いて DMD 患者および健常者について尿中 PGDM 濃度を測定し，DMD の病状診断に有効であるかどうかを検討した。

DMD はまだ治療法が確立していない難病で現在は病気の進行を遅らせる様々な試みがされている。この DMD の病態進行に PGD_2 を介した炎症が関係していることが明らかになり、26 年度は代表的な炎症マーカーのプロスタグランジン E2（PGE_2）も DMD に関与しているかを考察した。そこで DMD 患者の尿中の PGDM と PGEM を測定し、DMD の診断に有効であるかを検討した。

B．研究方法

［24 年度］

1) 対象

4～23 歳の DMD 患者 46 名および健常者 35 名を対象とした。

2) 測定用試料の調製

DMD 患者および健常者の尿 0.4ml に純水 0.5ml を加え、さらに内標準物質(tetranor-PGDM-d6)を加えて混和したのち, 1N HCl で pH3 程度に調整した。あらかじめエタノールと純水で洗浄した固相抽出カラム Sep-Pak Vac に全量をアプライした。5%アセトニトリル 6ml に続いてヘキサン 6ml で洗浄したのち、酢酸エチル 3ml で溶出した。この抽出液を窒素ガスで濃縮乾固したのち、10%アセトニトリル 100μl で再溶解して測定用試料とした。検量線作成のために内標準物質を加えた各濃度の標準試料についても同様に作成した。

図4にPGDM測定用試料の定量法のフローチャートを示す。

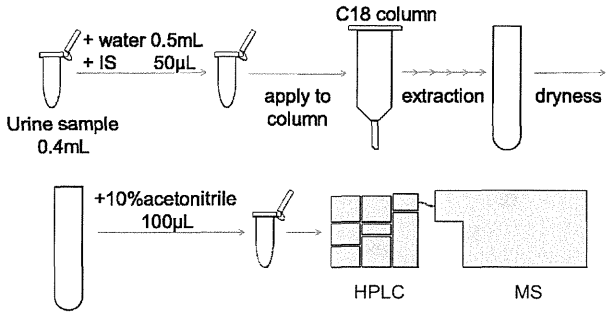

図4　PGDM測定用試料の定量法のフローチャート

3) LC-MS/MSによる測定

標準試料・測定用試料をAPI3000 LC-MS/MS systemに適用し，最適条件におけるプリカーサーおよびプロダクトイオンを検討した後，SRM法で測定した。PGDMと内標準物質とのピーク面積比を用いて定量値を算出した。

図5にLC-MS/MS測定に用いたHPLC並びにMS条件を示す。

また，比色定量により尿中クレアチニンを定量し，その定量値を補正に用いた。

HPLC	Shimadzu LC-10ADvp [SHIMADZU CORPORATION]
Column	Inertsil ODS-3 (5μm, 2.1mm I.D. × 150mm)
Mobile phase	A:0.01% acetic acid, B:acetonitrile
Gradient (B.conc)	0-2min 10%, 24min 30%, 27min 70%, 28min 100%, 31min 100%
Flow rate	0.25mL/min

MS	API3000 LC/MS/MS System [Applied Biosystems]
Ionization	Electrospray ionization (ESI)
Polarity	Negative ion mode
Duration	40min
Injection volume	20μL

図5　LC-MS/MS条件

［25年度］

1) 対象

2～55歳の患者1,003検体および2～14歳の健常者116検体、健常成人86検体を対象とした。

各種筋疾患患者の内訳は、DMD、BMD、γ-サルコグリカノパチー、ラミノパチー、先天性ミオパチー、B-ジストログリカン異常などである。

また、尿中PGDM濃度の日内変動を調べたところ、概して早朝に低く、日中に高い傾向が見られたことから、早朝一番尿を採取した。

2) 測定用試料の調製およびLC-MS/MSによる定量

患者および健常者の尿0.4mlに純水0.5mlを加え、さらに内標準物質(tetranor-PGDM-d6)を加えて混和したのち，1N HClでpH3程度に調整した。次に固相抽出カラムSep-Pak Vacを用いて抽出した。この抽出液を窒素ガスで濃縮乾固したのち、10%アセトニトリル100μlで再溶解して測定用試料とした。検量線作成のために内標準物質を加えた各濃度の標準試料についても同様に作成した。標準試料・測定用試料をAPI3000 LC-MS/MS systemに適用し，最適条件におけるプリカーサーおよびプロダクトイオンを検討した後，SRM（Selected Reaction Monitoring）法で測定した。PGDMと内標準物質とのピーク面積比を用いて定量値を算出した。また，比色定量によりクレアチニンを定量し，補正した。

［26年度］

1) 対象

前年度の尿中PGDM濃度の測定使用した2～55歳の患者（DMDおよびBMD）1,003検体および2～14歳の健常者116検体、健常成人86検体を対象とした。

尿中PGDM濃度の場合、早朝に低く、日中に高い傾向が見られたことから、尿中PGEM濃度の測定の場合も早朝一番尿を採取した。

2) 測定用試料の調製およびLC-MS/MSによる定量

患者および健常者の尿0.4mlに純水0.5mlを加え、さらに内標準物質(tetranor-PGDM-d6およびtetranor-PGEM-d6)を加えて混和したのち，1N HClでpH3程度に調整した。次に固相抽出カラムSep-Pak Vacを用いて抽出した。この抽出液を窒素ガスで濃縮乾固したのち、10%アセトニトリル100μlで再溶解して測定用試料とした。検量線作成のために内標準物質を加えた各濃度の標準試料についても同様に作成した。

標準試料・測定用試料をAPI3000 LC-MS/MS systemに適用し，最適条件におけるプリカーサーおよびプロダクトイオンを検討した後，SRM（Selected Reaction Monitoring）法で測定した。PGDMと内標準物質とのピーク面積比を用いて定量値を算出した。また，比色定量によりクレアチニンを定量し，補正した。

《HPLC測定条件》

装置:Shimadzu 10ADvp[Shimadzu]

カラム:Inertsil ODS-3 column
(150×2.1 mm i.d.) [GL Sciences]

移動相:

A;0.01%(v/v) acetic acid, B;acetonitrile

B:0-2min 10%,,24min 30%, 24min 70%, 28min

100%
流速:250μl/min

C．研究結果

［24 年度］

LC-MS/MS で高い選択性を有するプリカーサーおよびプロダクトイオンを用いることにより，PGDM は単一のピークとして認められ，微量定量が可能であった（図 6）。

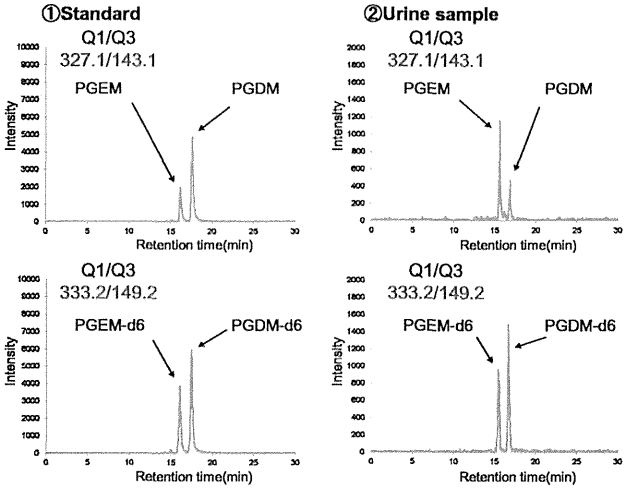

図 6　LC-MS/MS クロマトグラム

検量線も良好な直線性を示し，信頼性の高い定量ができたと判断した（図 7）。

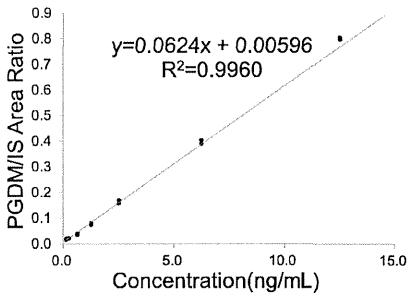

図 7　検量線

尿中 PGDM 濃度の日内変動を調べたところ、概して早朝に低く、日中に高い傾向が見られた（図 8）。この結果から、早朝尿を測定対象とすることにした。

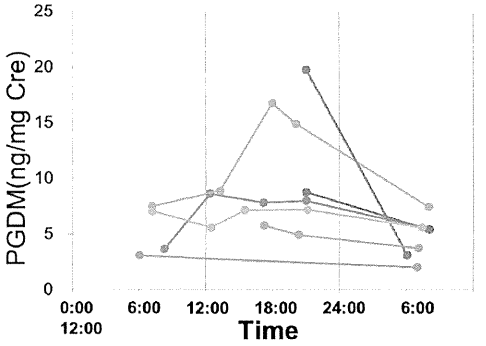

図 8　尿中 PGDM 濃度の日内変動

クレアチニン濃度で補正した尿中 PGDM 濃度を DMD 患者と健常者で比較したところ，DMD 患者の方が高かった（図 9）。

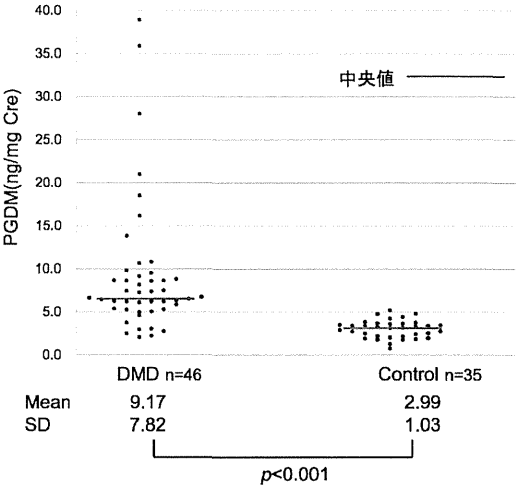

図 9　健常群、DMD 群の尿中 PGDM 濃度の分布

［25 年度］

2～55 歳の患者から採取した早朝一番尿 1,003 検体中の PGDM を測定したところ、健常者の尿に比べ、高かった。

各種筋疾患患者のうち、DMD と BMD を比較したところ、尿中 PGDM は DMD の方が有意に高かった。

DMD、BMD、γ-サルコグリカノパチー、ラミノパチー、先天性ミオパチー、B-ジストログリカン異常など他の筋疾患の尿中 PGDM を測定したところ、疾患により差が認められた。著しく高値を示す疾患があったが、検体数が少ないため今後の課題とし、検体数を増やして検討する必要がある。

［26 年度］

2～55 歳の患者から採取した早朝一番尿 1,003 検体中の尿中PGDMおよびPGEMを測定したところ、それぞれのピークは分離し、単一ピークとして検出され、分離定量が可能であった。

図 10 に示すように、尿中 PGDM 濃度および尿中 PGEM 濃度を DMD 患者と健常者で比較したと

き DMD 患者の方がともに数値が高かった。DMD と BMD を比較したところ、尿中 PGDM 濃度および尿中 PGEM 濃度は DMD の方が有意に高かった。

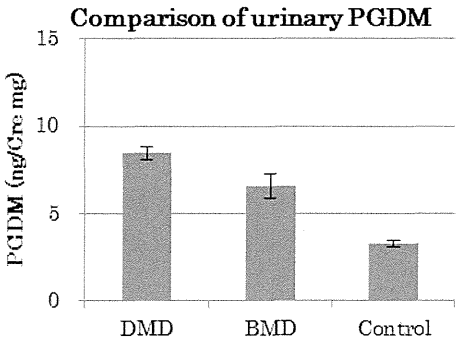

DMD vs BMD : $p<0.05$
DMD vs Control , BMD vs Control : $p<0.001$

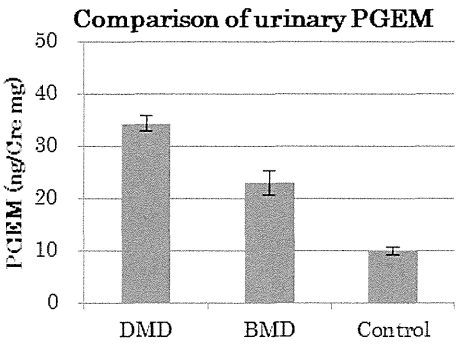

DMD vs BMD : $p<0.005$
DMD vs Control, BMD vs Control : $p<0.001$

図 10　健常群、DMD 群, BMD 群のの尿中 PGDM および PGEM 濃度の比較

症状から分類した年齢郡に分けて尿中 PGDM 濃度と尿中 PGEM 濃度の関係と検討したところ、いずれの年齢群においても相関が認められた。

年齢別に検討したところ、尿中 PGDM 濃度は症状との関係が認められたが、尿中 PGEM 濃度に関係が認められなかった。

D．考察

MS/MS による最適なプロダクトイオン，プリカーサーイオンを用いて SRM 法を行った結果，高い選択性により，PGDM は単一のピークとして認められた。また，IS とのピーク面積比を用いて算出した定量値も，検量線が良好な直線性を示したことから，信頼性の高い微量定量ができたと考えられた。

クレアチニン補正を行って算出した尿中 PGDM 濃度において，DMD 患者と健常者で比較したところ，DMD 患者の方が有意に高値であった。

PGDM 濃度は，早朝尿で評価すると随時尿よりも安定した結果が得られると考えられた。

DMD 患者および健常者について測定したところ、DMD の病状診断に有効である可能性が示唆された。また、他の筋疾患患者の尿中 PGDM を測定したところ、疾患により差が認められた。以上の結果より、治療効果の判定に応用可能であると考えられた。

DMD 患者では、筋繊維の壊死に伴って PGD_2 を介した炎症が起こり、PGDM の数値も上昇すると考えられる。これまで行ってきた DMD 患者および健常者中の尿中 PGDM 濃度測定の結果から、PGD_2 の代謝産物である尿中 PGDM 濃度は DMD の病状診断に有効であると判断された。

また、PGE_2 の代謝産物である PGEM 濃度は結果からは、必ずしも DMD の診断に有効であるとは言えず、今後も検討していく必要があると考えられた。

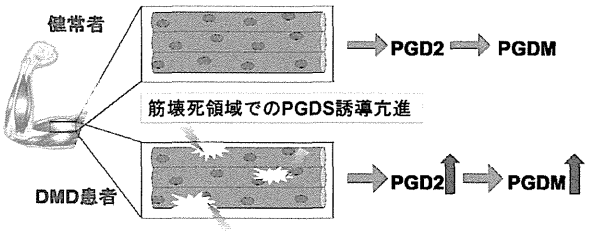

図 11　健常群、DMD 群における PGDM 生成

E．結論

API3000 LC/MS/MS system を用いる PGD_2 の代謝物である尿中 PGDM 濃度の測定法を確立した。

尿中 PGDM 濃度は、健常者＜BMD 患者＜DMD 患者の順に高かったことから、DMD の病状診断に有効であることが明らかとなった。

尿中 PGDM は DMD 濃度の病状診断に有効であるが、PGE_2 の代謝産物である PGEM 濃度は、必ずしも DMD の診断に有効であるとは言えないことが明らかとなった。

F．研究発表

1．論文発表

Nakagawa T, Takeuchi A, Kakiuchi R, Lee T, Yagi M, Awano H, Iijima K, Takeshima Y, Urade Y, Matsuo M.
"A prostaglandin D_2 metabolite is elevated in the urine of Duchenne muscular dystrophy patients and increases further from 8years old."
Clin. Chim. Acta. **2013** 423(23) 10-14.

2．学会発表

1) 垣内　涼平, 成田　哲也, 竹内　敦子, 裏出　良博, 鎌内　慎也, 松尾　雅文
「筋ジストロフィー患者の尿中プロスタグランジンD_2代謝物の定量」
日本薬学会第132年会 (2012.03.30 札幌).

2) Taku Nakagawa, Atsuko Takeuchi, Ryohei

Kakiuchi, Tomoko Lee, Mariko Yagi, Hiroyuki Awano, Kazumoto Iijima, Yasuhiro Takeshima, Yoshihiro Urade, Masafumi Matsuo
"A prostaglandin D_2 metabolite is elevated in the urine samples of patients with Duchenne muscular dystrophy"
18th International WMS Congress (2013. 10.1-5 Asilomar, California, USA)

3) 松尾　雅文，裏出　良博，竹内　敦子
「デュシェンヌ型筋ジストロフィーの尿中プロスタグランジン代謝産物解析」
第40回BMSコンファレンス（2013.7.9　宮崎）

4) 竹内　敦子，裏出　良博，松尾　雅文
「LC-MS/MSによるDuchenne型筋ジストロフィー患者の尿中プロスタグランジンD_2代謝物の定量」
第40回BMSコンファレンス（2013.7.9　宮崎）

5) 柳下　沙絢，竹内　敦子，中川　卓，竹島　泰弘，裏出　良博，松尾　雅文
「デュシェンヌ型筋ジストロフィー患者尿中プロスタグランジンD2代謝物濃度」
第61回質量分析総合討論会（2013.9.10　つくば）

5) Atsuko Takeuchi
"LC-MS/MS quantification of a prostaglandin D_2 metabolite in the urine of Duchenne muscular dystrophy patients"
Japan-Vietnam joint research meeting on Duchenne muscular dystrophy (2014.2.26　Hanoi, Vietnam)

6)竹内敦子
「疾患の診断・治療をめざす質量分析の応用研究」
第 67 回日本臨床化学会近畿支部例会（2014.6.14 神戸）

7) 藤井 菜摘，竹内 敦子，裏出 良博，松尾 雅文
「筋ジストロフィー患者の尿中プロスタグランジン代謝物（tetranor-PGDMおよびtetranor-PGEM）の定量」
日本薬学会第135年会（2015.3.26　神戸）

G．知的財産権の出願・登録状況
特になし

研究成果の刊行に関する一覧表

書籍

著者氏名	論文タイトル名	書籍全体の編集者名	書　籍　名	出版社名	出版地	出版年	ページ
裏出良博	筋ジストロフィー患者の尿中プロスタグランジン代謝物の定量	松嶋正明、伊中浩治	進化をとげる構造生物学	株式会社化学同人	東京	2014	169-180

雑誌

発表者氏名	論文タイトル名	発表誌名	巻号	ページ	出版年
Trimarco A, Forese MG, Alfieri V, Lucente A, Brambilla P, Diana G, Pieragostino D, Sacchetta P, Urade Y, Boizet-Bonhoure B, Martinelli Boneschi F, Quattrini A, Taveggia C	Prostaglandin D_2 synthase/GPR44: a signaling axis in PNS myelination	Nat Neurosci	17(12)	1682-92	2014
Asai.T.,Ojima.I., Minami.S., Takeshima.Y., Matsuo.M.,	Gait training for becker's muscular dystrophy using robot suit hybrid assistive limb	Physical Medicine and Rehabilitation-International	1	1-3	2014
Izumi Y, Aritake K, Urade Y, Fukusaki	Practical evaluation of liquid chromatography/tandem mass spectrometry and enzyme immunoassay method for the accurate quantitative analysis of prostaglandins	J Biosci Bioeng	118(1)	116-8	2014
Sarashina H, Tsubosaka, Y, Omori K, Aritake K, Nakagawa M, Hori M, Hirai H, Nakamura M, Narumiya S, Urade Y, Ozaki H, Murata T	Opposing immunomodulatory roles prostaglandin D_2 during the progression of skin inflammation	J Immunol	192	459-465	2014
Maekawa K, Hirayama A, Iwata Y, Tajima Y, Nishimaki-Mogami T, Sugawara S, Ueno N, Abe H, Ishikawa M, Murayama M, Matsuzawa Y, Nakanishi H, Ikeda K, Arita M, Taguchi R, Minamino N, Wakabayashi S, Soga T, Saito Y	Global metabolic analysis of heart tissue in a hamster model for dilated cardiomyopathy	J. Mol. Cell Cardiol.	59	76-85	2013

Iwata Y, Ohtake H, Suzuki O, Matsuda J, Komamura K, Wakabayashi S	Blockade of sarcolemmal TRPV2 accumulation inhibits progression of dilated cardiomyopathy	Cardiovas. Res	99	760-768	2013
Nakagawa T, Takeuchi A, Kakiuchi R, Lee T, Yagi M, Awano H, Iijima K, Takeshima Y, Urade Y, Matsuo M	A prostaglandin D_2 metabolite is elevated in the urine of Duchenne muscular dystrophy patients and increases further from 8years old	Clin. Chim. Acta	423(23)	10-14	2013
Taketomi Y, Ueno N, Kojima T, Sato H, Murase R, Yamamoto K, Tanaka S, Sakanaka M, Nakamura M, Nishito Y, Kawana M, Kambe N, Ikeda K, Taguchi R, Nakamizo S, Kabashima K, Gelb M H, Arita M, Yokomizo T, Nakamura M, Watanabe K, Hirai H, Nakamura M, Okayama Y, Ra C, Aritake K, Urade Y, Morimoto K, Sugimoto Y,Shimizu T, Narumiya S, Hara S, Murakami M.	Mast cell maturation is driven via a grouop III Phospholipase A_2-Prostaglandin D_2-DP I receptor paracrine axis	Nat Immunol	14(6)	554-563	2013
Iwata Y, Suzuki O, Wakabayashi S	Decreased surface sialic acid content is a sensitive indicator for muscle damage	Muscle & Nerve	47	372-378	2013
Murata, T., Aritake,K., Tsubosaka,Y., Maruyama, T., Nakagawa,T., Hori, M., Hirai, H., Nakamura, M. Narumiya, S., Urade, Y., Ozaki, H.	Anti-inflammatory role of PG D_2 in acute lung inflammation and therapeutic application of its signal enhancement	Proc Natl Acad Sci U S A	110 (13)	5205-10	2013

学会発表

発表者氏名	演題名	学会名	年度
藤井 菜摘, 竹内 敦子, 裏出 良博, 松尾 雅文	筋ジストロフィー患者の尿中プロスタグランジン代謝物（tetranor-PGDMおよびtetranor-PGEM）の定量	日本薬学会第135年会、神戸	2015年3月
裏出　良博	筋ジストロフィー患者のリハビリーテーションに用いる尿中マーカー物質の測定法	障害者対策事業成果発表、東京	2015年2月
裏出　良博	筋ジストロフィー病態の進行軽減療法開発	筋ジストロフィー合同班会議、東京	2015年1月
Tanaka K, Aritake K, Tayama M, Sasaki E, Utsugi T, A Sasaoka T, URADE Y	Novel inhibitor of hematopoeietic prostaglandin D synthase improves the muscle disorder in an experimental model of Duchenne muscular dystrophy	International Congress of the world muscle Society (WMS2014), Germany	2014年10月
Tanaka K, Aritake K, Tayama M, Shigeno K, Hayashi Y, Sasaki E, Utsugi T,Sasaoka T, Urade Y	Inhibition of hematopoietic prostaglandin D synthase improves sympotoms of muscular dystrophy in a mouse model of Duchenne muscular dystrophy	NEUROSCIENCE 2014, USA	2014年11月
駒村和雄、岩田裕子	拡張型心筋症の新規治療薬の開発:伸展感受性Ca透過型陽イオンチャネルTRPV2の阻害薬の可能性	第62回日本心臓病学会学術集会、仙台	2014年9月
Iwata, Y, Komamura, K	Transient Receptor Potential Vanilloid 2 Antagonist, Ameliorates End-Stage Heart Failure of Mice With Dilated Cardiomyopathy.	AHA Scientific Sessions 2014, USA	2014年11月
岩田裕子、大武仁美	TRPV2阻害剤によりマウス重症心筋症の進行が抑制される。	第86回日本生化学会大会、京都	2014年10月
竹内敦子	疾患の診断・治療をめざす質量分析の応用研究	第 67 回日本臨床化学会近畿支部例会、神戸	2014 年 6 月
鎌内慎也、岩田裕子、Cheng-Kun Du、Dong-Yun Zhan、森本幸生、白井幹康、若林繁夫	TRPV2 N 末ドメインの高発現は、トロポニン T 変異を持つ拡張型心筋症モデルマウスの症状を改善する	第 87 回日本薬理学会年会、仙台	2014 年 3 月

岩田裕子、大武仁美、鎌内慎也、若林繁夫	Ca2+透過チャネル TRPV2 の細胞膜局在の阻害により拡張型心筋症モデル動物の病態進行が抑制された。	第 87 回日本薬理学会年会、仙台	2014 年 3 月
Masafumi Matsuo	DMD treatment: overview" Japan-Vietnam joint research meeting on Duchenne muscular dystrophy	Japan-Vietnam joint research meeting on Duchenne muscular dystrophy	2014年2月
Masafumi Matsuo	Mutations in the dystrophin gen	Japan-Vietnam joint research meeting on Duchenne muscular dystrophy	2014年2月
Yoshiro Urade	Development of drugs used for therapy of Duchenne muscular dystrophy : Inhibitors of hemato-poietic prostaglandin D_2 synthase	Japan-Vietnam joint research meeting on Duchenne muscular dystrophy	2014年2月
Atsuko Takeuchi	LC-MS/MS quantification of a prostaglandin D_2 metabolite in the urine of Duchenne muscular dystrophy patients	Japan-Vietnam joint research meeting on Duchenne muscular dystrophy	2014年2月
Taku Nakagawa, Atsuko Takeuchi, Ryohei Kakiuchi, Tomoko Lee, Mariko Yagi, Hiroyuki, Awano, Kazumoto Iijima, Yasuhiro Takeshima, Yoshihiro Urade, Masafumi Matsuo	A prostaglandin D_2 metabolite is elevated in the urine samples of patients with Duchenne muscular dystrophy	18th International WMS Congress (2013. Asilomar, California, USA	2013年10月
岩田裕子、若林繁夫	Prostaglandin D_2 metabolites are elevated in the urine of animal models of dilated cardiomyopathy	第 86 回日本生化学会大会、横浜	2013 年 9 月
裏出良博、中川　卓、竹内敦子、垣内涼平、Tomoko Lee、八木麻里子、粟野宏之、飯島一誠、竹島泰弘、松尾雅文、有竹浩介	デュシェンヌ型筋ジストロフィーの新規病態マーカーとしての尿中 PGD_2 代謝物」	第 86 回日本生化学会大会、横浜	2013 年 9 月

有竹浩介、田中克尚、鈴木比佐子、三好和久、林　勧生、佐々木英治、裏出良博	Effect of a highly selective inhibitor for hematopoietic prostaglandin D synthase on an experimental model of Duchenne muscular dystrophy	第 86 回日本生化学会大会、横浜	2013 年 9 月
柳下　沙絢，竹内　敦子，中川　卓，竹島　泰弘，裏出　良博，松尾　雅文	デュシェンヌ型筋ジストロフィー患者尿中プロスタグランジンD2代謝物濃度	第61回質量分析総合討論会、つくば	2013年9月
有竹浩介、田中克尚、鈴木比佐子、三好和久、林　勧生、佐々木英治、裏出良博	Effect of a highly selective inhibitor for hematopoietic prostaglandin D synthase on an experimental model of Duchenne muscular dystrophy	第 86 回日本生化学会大会、横浜	2013 年 9 月
Yoshiro Urade	Use of protein crystal growth technology in space to discover and develop therapeutic candidates for Duchenne muscular dystrophy	2nd Annual ISS research and development conference, USA	2013年7月
松尾　雅文，裏出　良博，竹内　敦子	デュシェンヌ型筋ジストロフィーの尿中プロスタグランジン代謝産物解析	第 40 回 BMS コンファレンス、宮崎	2013 年 7 月
竹内　敦子，裏出　良博，松尾　雅文	LC-MS/MS による Duchenne 型筋ジストロフィー患者の尿中プロスタグランジン D_2 代謝物の定量	第 40 回 BMS コンファレンス、宮崎	2013 年 7 月
岩田裕子、若林繁夫	拡張型心筋症モデル動物におけるプロスタグランジン D_2 尿中代謝物の増加	第 86 回日本薬理学会年会、福岡	2013 年 3 月
岩田　裕子、若林繁夫	筋細胞膜の低下したシアール酸含量は筋変性疾患における傷害の高感度マーカーである	第86回日本薬理学会年会、福岡	2013 年 3 月
岩田　裕子	Inhibition of Ca2+-permeable channel TRPV2 provides the beneficial effects on cardiomyopathy	第9回日仏国際シンポジウム、東京	2012年9月
垣内　涼平，成田　哲也，竹内　敦子，裏出　良博，鎌内　慎也，松尾雅文	筋ジストロフィー患者の尿中プロスタグランジンD_2代謝物の定量	日本薬学会第132年会、札幌	2012年3月

特許権等の知的財産権の出願・登録状況

氏名	題名	番号	取得日
岩田　裕子、若林　繁夫	TRPV2阻害剤、疾患の予防又は治療剤、薬剤探索用リード化合物、及び薬剤探索方法	特許第5667223号	2014年12月19日
岩田　裕子、若林　繁夫	TRPV2の部分ペプチド	特許第5644026号	2014年11月14日
鈴木　治、岩田　裕子	筋傷害の簡便検査方法及び筋傷害検査用キット	特許第4997441号	2012年5月25日

その他

発表内容	題名	年度
ボーイング社ホームページ掲載	日本人科学者　裏出博士の筋ジストロフィー治療薬の開発	2014年3月
第32回全国筋ジストロフィー大阪大会 基調講演：　裏出　良博	デュシェンヌ型筋ジストロフィーの薬物療法	2014年10月
大鵬薬品工業㈱登録番号（NCT02246478）臨床試験開始 *米国NIH広報	H-PGDS阻害薬（TAS-205）を用いたDMD患者を対象とした臨床試験	2014年9月

nature neuroscience

Prostaglandin D2 synthase/GPR44: a signaling axis in PNS myelination

Amelia Trimarco[1,2], Maria Grazia Forese[1,2], Valentina Alfieri[1,2], Alessandra Lucente[1,2], Paola Brambilla[1,2], Giorgia Dina[1,2], Damiana Pieragostino[3], Paolo Sacchetta[3], Yoshihiro Urade[4], Brigitte Boizet-Bonhoure[5], Filippo Martinelli Boneschi[1,2], Angelo Quattrini[1,2] & Carla Taveggia[1,2]

Neuregulin 1 type III is processed following regulated intramembrane proteolysis, which allows communication from the plasma membrane to the nucleus. We found that the intracellular domain of neuregulin 1 type III upregulated the prostaglandin D2 synthase (*L-pgds*, also known as *Ptgds*) gene, which, together with the G protein–coupled receptor Gpr44, forms a previously unknown pathway in PNS myelination. Neuronal L-PGDS is secreted and produces the PGD2 prostanoid, a ligand of Gpr44. We found that mice lacking L-PGDS were hypomyelinated. Consistent with this, specific inhibition of L-PGDS activity impaired *in vitro* myelination and caused myelin damage. Furthermore, *in vivo* ablation and *in vitro* knockdown of glial Gpr44 impaired myelination. Finally, we identified Nfatc4, a key transcription factor for myelination, as one of the downstream effectors of PGD2 activity in Schwann cells. Thus, L-PGDS and Gpr44 are previously unknown components of an axo-glial interaction that controls PNS myelination and possibly myelin maintenance.

Glial cells, oligodendrocytes in the CNS and Schwann cells in the PNS, wrap around axons to form myelin, which is essential for rapid conduction of electrical impulses and neuronal survival. In the PNS, the levels of axonal neuregulin 1 (NRG1) type III, a member of the NRG family of growth factors, controls all aspects of Schwann cell development and myelin formation[1]. We recently found that NRG1 type III activity is modulated by competitive extracellular cleavage between the beta secretase BACE-1 (refs. 2,3) and the alpha secretase TACE (Adam17)[4].

NRG1 type III is also intramembrane processed by the γ-secretase complex following a classically regulated intramembrane proteolysis cleavage, suggesting that it might function as a bidirectional molecule[5]. Previous studies showed that, in hippocampal neurons, this cleavage event is regulated by the erbB receptors and generates an intracellular domain that represses the expression of pro-apoptotic genes *in vitro*[5]. In the mouse cochlea, the NRG1 intracellular domain can be further processed to generate a smaller fragment that enhances the expression of PSD95 (Dlg4)[6]. Finally, mutations in the putative transmembrane cleavage domain of NRG1 alter the branching of cortical dendrites[7].

We report that NRG1 type III undergoes a similar intramembrane processing in the PNS, but, unlike previous studies, we found that the generated fragment upregulated the prostaglandin D2 synthase (*L-pgds*) gene. L-PGDS, an *N*-glycosylated protein that is highly expressed in several tissues[8], is part of the prostaglandin synthase' family of proteins and controls many biological events. L-PGDS can be secreted[9,10] and functions as an enzyme or as an extracellular transporter of lipoliphic molecules[11]. Prostaglandins are generated by the processing of arachidonic acid and have been mainly implicated in inflammation. Following release by phospholipase A, arachidonic acid binds to the catalytic site of the COX enzymes (Cox-1 and Cox2) to generate the intermediate prostaglandin H2 (PGH2)[12,13]. Several synthases, including L-PGDS, convert this metabolite into different prostaglandins. L-PGDS catalyzes the conversion of PGH2 into the functional prostaglandin D2 (PGD2). PGD2 is also synthesized by the hematopoietic prostaglandin D synthase (*H-pgds*, also known as *Ptgds2*), which is expressed in inflammatory cells and in microglial cells[8]. PGD2 can be further dehydrated to PGJ2. 15d-PGJ2, the final non-enzymatic product of PGD2 dehydration, has a variety of biological actions, including neurotoxic and neuroprotective properties[13,14]. PGD2 and PGJ2 can bind Gpr44 and Ptgdr, members of the G protein–coupled receptor family, and the nuclear receptor Pparg[15], respectively. After binding, they activate intracellular signaling responses that vary depending on the type of receptor initially stimulated[16]. In particular, PGD2 modulates intracellular messengers such as calcium, cAMP and phosphoinositol concentrations[15,17].

We found that intracellular cleavage and nuclear translocation of NRG1 type III in the PNS induced the expression of L-PGDS and the activation of Gpr44, which contribute to myelin formation and maintenance. Inhibition of L-PGDS activity *in vitro* impaired PNS myelination. Accordingly, sciatic nerves of *L-pgds*$^{-/-}$ transgenic mice were hypomyelinated. We also found that H-PGDS was expressed in nerves, but was dispensable for myelination. Notably,

[1]Division of Neuroscience, San Raffaele Scientific Institute, Milan, Italy. [2]INSPE at San Raffaele Scientific Institute, Milan, Italy. [3]Department of Experimental and Clinical Sciences, University "G. D'Annunzio", Chieti, Italy. [4]International Institute for Integrative Sleep medicine, University of Tsukuba, Ibaraki, Japan. [5]Institut de Génétique Humaine CNRS UPR1142, Montpellier, France. Correspondence should be addressed to C.T. (taveggia.carla@hsr.it).

Received 23 July; accepted 7 October; published online 2 November 2014; corrected online 17 November 2014 (details online); doi:10.1038/nn.3857

H-pgds $^{-/-}$*; L-pgds*$^{-/-}$ mice were hypomyelinated and the myelin sheath was aberrant in aged animals. Furthermore, we found that PGD2, the product of L-PGDS enzymatic activity, most likely signals through the Gpr44 receptor onto Schwann cells, as glial-specific knockdown of Gpr44 impaired *in vitro* myelination. *Gpr44*$^{-/-}$ transgenic mice were hypomyelinated in the PNS. Finally, activation of Gpr44 led to dephosphorylation of the transcription factor Nfatc4 (ref. 18), indicating that it is a downstream effector of L-PGDS activity.

We propose that L-PGDS and the G protein–coupled receptor Gpr44 are modulators of PNS myelination. Our findings suggest that NRG1 type III controls myelination in multiple ways and our data support the existence of a previously unknown pathway whose modulation could be beneficial for the treatment of peripheral demyelinating neuropathies. To the best of our knowledge, these results are the first to implicate prostaglandins as active controllers of myelination.

RESULTS

NRG1 type III is cleaved by γ-secretase and activates L-PGDS

To investigate whether NRG1 type III intracellular cleavage occurs in PNS neurons, we generated two lentiviral vectors expressing NRG1 type III tagged with an EGFP epitope at either the N-terminal (N-NRG1) or C-terminal end (C-NRG1). We then infected rat primary dorsal root ganglia (DRG) neurons and found that N-NRG1 (data not shown) and C-NRG1 were similarly expressed in axons. However, C-NRG1 was no longer present following Schwann cell contact (**Fig. 1a**). Notably, addition of 10 μM γ-secretase specific inhibitor Compound E[19] maintained the expression of the EGFP epitope in the axons (**Fig. 1a**), suggesting that the C-terminal end of NRG1 type III undergoes a γ-secretase–dependent cleavage, which is also Schwann cell dependent.

To determine whether the generated NRG1 type III fragment translocates into the nucleus, we infected rat primary DRG neurons with a lentiviral construct expressing the constitutively cleaved form of NRG1 type III tagged with a FLAG epitope at the C terminus (NRG1 ICD). Immunofluorescence analyses revealed that the FLAG epitope was present in nuclei of DRG infected neurons (**Fig. 1b**). We observed NRG1 ICD staining in approximately 78% of DRG neurons, 66.2% ± 18.8 of which expressed nuclear FLAG (four different infections, at least three coverslips per infection).

Despite this result, the conditions of our experiment were not physiologically realistic due to the expression of the already processed fragment. Thus, to assess whether NRG1 ICD physiologically translocates, we infected DRG neurons with a lentivirus expressing full-length NRG1 type III tagged with a FLAG epitope at the C terminus. Our initial finding implicated Schwann cells in the intracellular processing of full-length NRG1 type III. Thus, 7 d after infection, we added rat primary Schwann cells to DRG neurons and we examined FLAG localization by immunofluorescence. As expected, we detected the FLAG epitope in the nuclei of infected DRG neurons (**Fig. 1c**), confirming that NRG1 type III physiologically undergoes classical intramembrane proteolysis.

To evaluate whether NRG1 ICD nuclear translocation modifies gene transcription, we performed genome-wide expression analysis on an Illumina platform. We compared mRNA expression levels of DRG

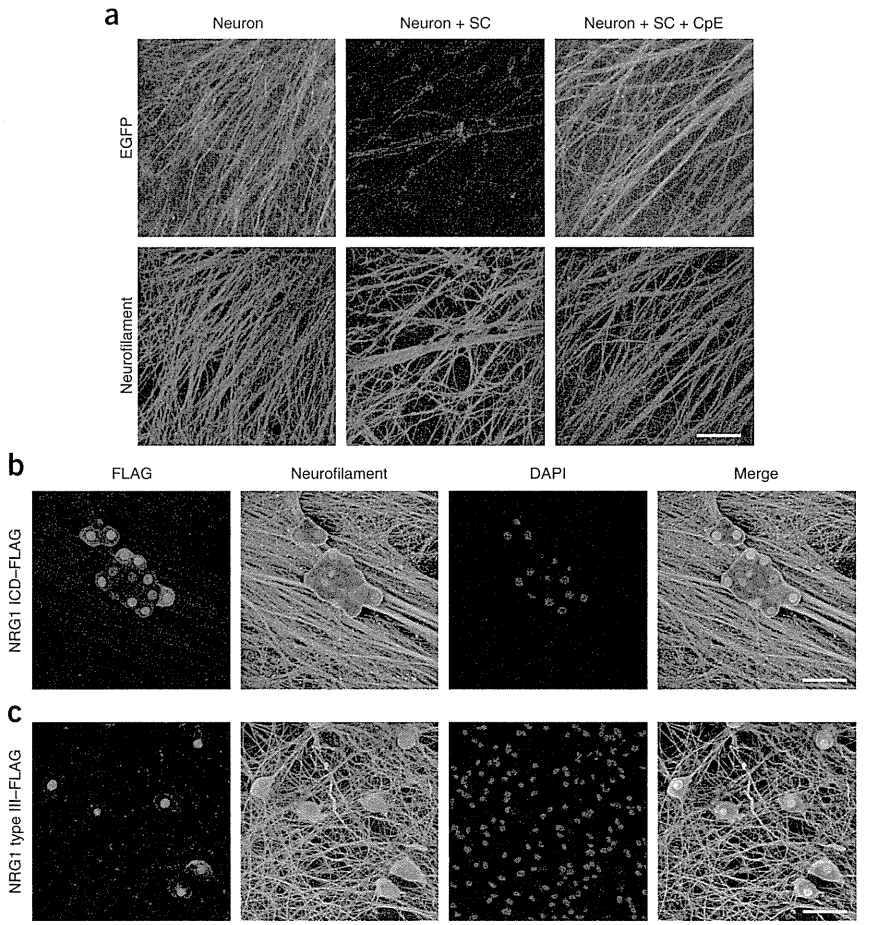

Figure 1 NRG1 type III undergoes a regulated intramembrane proteolysis cleavage that is Schwann cell dependent. (**a**) Rat DRG neurons infected with full-length NRG1 type III, tagged at the C terminus with EGFP, were stained for GFP (fluorescein) and neurofilament (rhodamine). The addition of Schwann cells induced clearance while in the presence of 10 μM Compound E (CpE). EGFP expression remained associated to the axons. The images are representative of three different independent experiments ($N = 3$ infections performed with different viral stock preparation onto different neuronal cultures). Scale bar represents 100 μm. (**b**) Rat DRG neurons were infected with a lentivirus expressing NRG1 ICD tagged with a FLAG epitope at the C terminus. The FLAG tag (rhodamine) was expressed in the nuclei, as shown by colocalization with nuclear staining (DAPI, blue). Neurofilament staining is also indicated (fluorescein). The images are representative of three different independent experiments ($N = 3$ infections performed with different viral stock preparation onto different neuronal cultures). Scale bar represents 100 μm. (**c**) Rat DRG neurons were infected with a lentivirus expressing full-length NRG1 type III tagged with a FLAG epitope at the C terminus. In the presence of Schwann cells, the FLAG tag (rhodamine) was expressed in the nuclei, as shown by colocalization with nuclear staining (DAPI, blue). Neurofilament staining is also indicated (fluorescein). The images are representative of three different independent experiments ($N = 3$ infections performed with different viral stock preparation onto different neuronal cultures). Scale bar represents 100 μm.

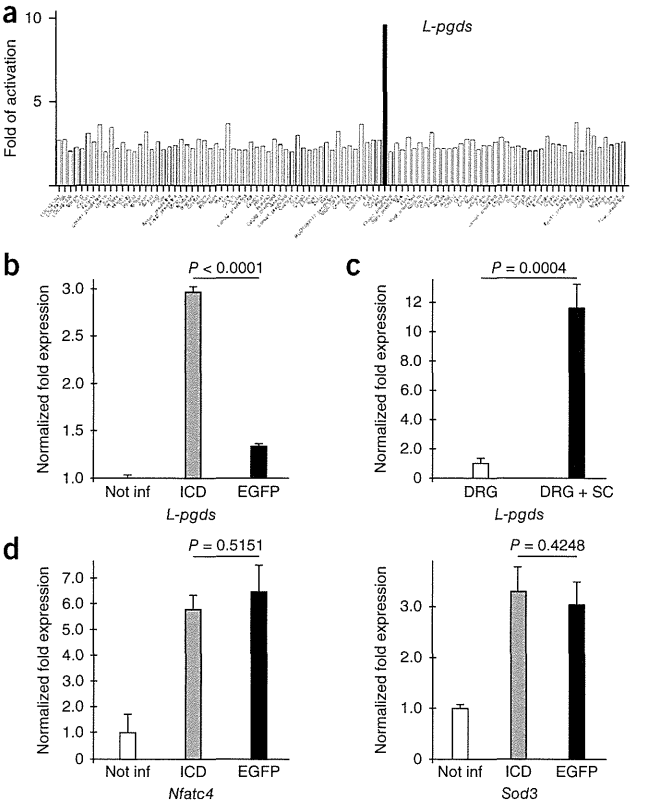

Figure 2 *L-pgds* is the most upregulated gene in neurons infected with NRG1 ICD. (**a**) Graph indicating all genes that were significantly upregulated in the Illumina analyses in NRG1 ICD–infected neurons compared with uninfected neurons. *L-pgds* showed a nine-fold change of activation (Limma moderated *t* test, $P = 0.00015$, $t = 5.25$, df = 6). $N = 4$ different independent RNA preparations and analyses. The complete list of upregulated genes is reported in **Supplementary Table 1**. (**b**) *L-PGDS* was upregulated only in neurons overexpressing NRG1 ICD. qRT-PCR analyses of mRNA prepared from DRG neurons not infected or infected with a lentivirus expressing either NRG1 ICD or EGFP confirmed specific upregulation of *L-pgds* in DRG neurons expressing NRG1 ICD. Data have been normalized to *Gapdh* expression level. Data were analyzed with the CFX Manager Software (Biorad) (one-way ANOVA, $***P \leq 0.0001$ NRG1 ICD versus EGFP (ICD – EGFP), $F = 706$). Error bars represent mean ± s.e.m. Graph is representative of three different independent experiments. $N = 3$ different RNA preparations and analyses. (**c**) Neuronal *L-PGDS* expression was upregulated in DRG neurons following the addition of Schwann cells. qRT-PCR analyses of mRNA prepared from purified mouse DRG neurons and mouse DRG neurons seeded with rat primary Schwann cells are shown. Amplification with primers specifically designed for mouse *L-pgds*, which do not amplify the rat *L-pgds* sequence, confirmed that neuronal *L-pgds* expression was induced by Schwann cell contact. Data are normalized to *Gapdh* expression level (*t* test analysis, $P = 0.0004$, $t = 10.8$, df = 4). Error bars represent mean ± s.d. Shown graph is representative of three different independent experiments. $N = 3$ different RNA preparations and analyses. (**d**) qRT-PCR analyses of mRNA prepared from DRG neurons not infected or infected with a lentivirus expressing either NRG1 ICD or EGFP to test the expression of genes that in the Illumina screening were upregulated above threshold. Upregulation of *Nfatc4* and *Sod3* was not specific, as it is also present in EGFP-infected DRG neurons. Data were analyzed with the CFX Manager Software on three mRNA different preparations (one-way ANOVA: *Sod3*, $P = 0.5151$ ICD – EGFP, $F = 30.95$; *Nfatc4*, $P = 0.4248$ ICD – EGFP, $F = 40.42$). Error bars represent mean ± s.d. Shown graphs are representative of three different independent experiments. $N = 3$ different RNA preparations and analyses.

neurons infected with a lentivirus expressing NRG1 ICD, not infected or infected with a lentivirus expressing EGFP as controls. Of the genes upregulated with a fold change cut-off of 2.0 ($P < 0.01$), *L-pgds* was the most upregulated in DRG neurons overexpressing NRG1 ICD (**Fig. 2**, **Supplementary Fig. 1a**,**b** and **Supplementary Table 1**).

We next confirmed upregulation of *L-pgds* by RT-PCR (**Supplementary Fig. 1c**) and quantitative RT-PCR (qRT-PCR) analyses (**Fig. 2b**) of mRNA prepared from DRG neurons infected as described above. In addition, we validated these results by determining mRNA levels of *Nfatc4* and *Sod3*, two genes whose expression was above threshold. As expected, we observed that the latter were not exclusively upregulated in NRG1 ICD–infected neurons (**Fig. 2d**). Furthermore, we found that *L-pgds* mRNA expression was increased in mouse DRG neurons only when co-cultured in the presence of rat primary Schwann cells, suggesting that the physiological interaction of Schwann cells with DRG neurons induced *L-pgds* expression (**Fig. 2c**). These results strongly indicate that NRG1 type III intracellular processing induces a specific activation of *L-pgds* mRNA in DRG neurons that is Schwann cell dependent.

L-PGDS is released in the extracellular media

Our results suggest that intracellular processing of NRG1 type III activates the transcription of *L-pgds*, but do not provide any indication as to protein expression or its possible role in PNS. To determine whether L-PGDS protein is also upregulated with its mRNA, we measured L-PGDS protein levels by western blotting and by mass spectrometry shotgun analyses in lysates prepared from NRG1 ICD–infected neurons. To our surprise, we were not able to detect it (**Supplementary Fig. 2a** and data not shown), strongly suggesting that *L-pgds* mRNA is not translated or that the protein is quickly degraded or released into the extracellular media, as previously reported[20,21].

To assess whether L-PGDS protein is released by DRG neurons, we grew both NRG1 ICD–infected and not infected neurons in neurobasal media. We then collected the media after 48 h (**Fig. 3**) and determined L-PGDS expression by western blot. As expected, we detected L-PGDS protein in the conditioned media of neurons infected with NRG1 ICD (**Fig. 3a** and **Supplementary Fig. 2c**) or L-PGDS (**Supplementary Fig. 2b**), but we also detected a very limited amount of L-PGDS in the conditioned media of not infected DRG neurons, indicating that L-PGDS could be constitutively released and that its synthesis is upregulated by NRG1 ICD. We next sought to investigate the functional role of released L-PGDS. Given that L-PGDS is secreted via exosomes[22], we first determined whether Schwann cells could take it up. We grew purified primary rat Schwann cells in the presence of conditioned media prepared from DRG neurons infected with NRG1 ICD and analyzed L-PGDS expression in Schwann cells lysates by western blotting. Unlike the media, which retained L-PGDS expression, we never observed L-PGDS in Schwann cells lysates (**Fig. 3b** and **Supplementary Fig. 2c**).

Given that L-PGDS catalyzes the formation of prostaglandins, we determined whether it is enzymatically active in the extracellular media. Using liquid chromatography tandem mass spectrometry (LC-MS/MS), we measured the amount of PGD2, an L-PGDS metabolite, in conditioned media of DRG neurons that were either not infected or were infected with NRG1 ICD or EGFP. Only the conditioned media of neurons overexpressing NRG1 ICD accumulated PGD2. Notably, the conditioned media of DRG neurons infected with NRG1 ICD and cultured in the presence of AT-56, a specific L-PGDS

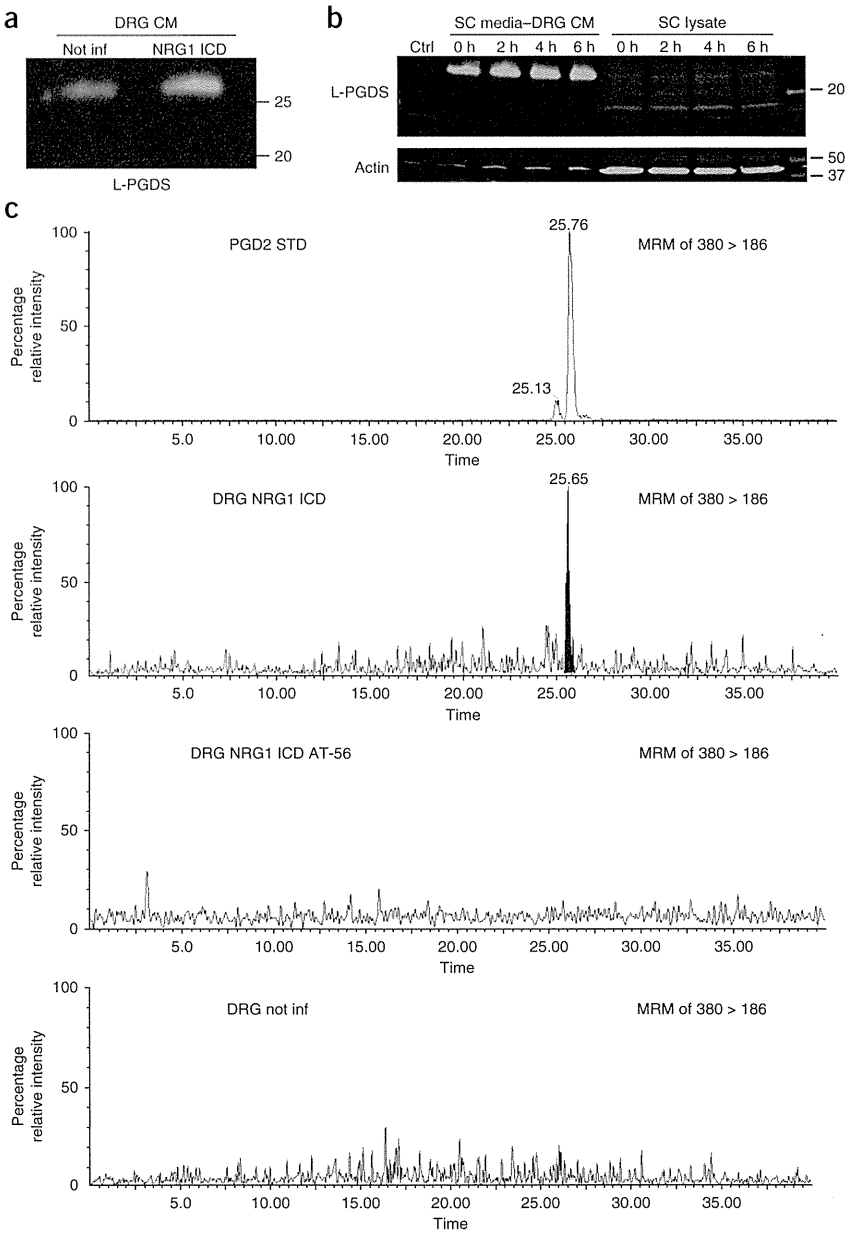

Figure 3 L-PGDS is secreted and enzymatically active. (**a**) Representative western blotting analyses of centrifuged DRG conditioned media (CM) from not infected or NRG1 ICD–infected DRG neurons. Cultures were infected the day after dissection, purified of endogenous Schwann cells (SCs) and grown for additional 14 d to allow lentivirus expression. Neurons were then grown in the presence of neurobasal media for additional 48 h, after which the media was tested for L-PGDS expression. L-PGDS was present in all samples and its levels were increased in NRG1 ICD–infected neurons. $N = 3$ independent experiments. (**b**) Conditioned media of DRG neurons infected with a lentivirus encoding for NRG1 ICD was prepared as in **a**. Primary rat Schwann cells were grown in the presence of collected DRG media for 2, 4 or 6 h, after which Schwann cells were lysed and tested for L-PGDS uptake by western blot. L-PGDS protein was not detected in Schwann cell lysates. Actin served as a control and was mainly present in lysates. The little amount of actin present in DRG conditioned media was probably a result of dead Schwann cells present in the supernatant. Regular Schwann cell growth media was used as a control. The image is representative of three different independent experiments. (**c**) PGD2 was detected by LC-MS/MS in conditioned media of DRG neurons overexpressing NRG1 ICD and in standard solution of PGD2, whereas, in conditioned media of wild-type DRG neurons, PGD2 was undetectable. Note that PGD2 did not accumulate in conditioned media of DRG neurons overexpressing NRG1 ICD treated with AT-56, a specific PGD2 inhibitor. Chromatograms are representative of three different experiments. For uncropped pictures of western blots, see **Supplementary Figure 10**. $N = 3$ conditioned media preparations.

inhibitor[23], did not accumulate PGD2 (**Fig. 3c** and **Supplementary Fig. 2e**). In conclusion, our results indicate that L-PGDS is released into the extracellular media, where maintains its enzymatic activity, as it was able to process PGH2 into PGD2.

L-pgds$^{-/-}$ sciatic nerves are hypomyelinated

PGD2 is the product of two different enzymes, H-PGDS, which is essentially expressed in inflammatory cells and in microglial cells, and L-PGDS, whose expression is enriched in brain[8] and sensory neurons[24]. To confirm the role of L-PGDS in myelination, we analyzed nerve morphology in *L-pgds*$^{-/-}$ mice. These mice display various abnormalities, including glucose intolerance and insulin resistance[25], sleep inhibition[26], acceleration of beta-amyloid deposition[27], and aberrant Sertoli cells maturation[28].

We analyzed sciatic nerves morphology in 1-month-old (**Fig. 4a–c**) and 6-month-old (**Fig. 4d–f**) *L-pgds*$^{-/-}$ mice. At both ages, myelin in *L-pgds*$^{-/-}$ sciatic nerves was noticeably thinner than that of wild-type mice. Morphometric analyses confirmed a significant increase in *g* ratio (axon diameter versus fiber diameter) in *L-pgds*$^{-/-}$ mice versus wild-type littermates (**Supplementary Table 2**) across a range of fibers, whereas axon diameters in adult nerves were comparable in 1-month-old mice and slightly increased in 6-month-old *L-pgds*$^{-/-}$ nerves. We also determined whether a lack of L-PGDS impaired Schwann cells development. We did not find any alteration in the expression of Pou3f1 (Oct6, Scip, Tst1) and Egr2 (Krox-20) or in Schwann cell survival and proliferation in postnatal day 2 (P2) *L-pgds*$^{-/-}$ nerves (**Supplementary Table 3**).

Next, we assessed H–PGDS expression in PNS. Immunohistochemical analyses showed that H-PGDS was expressed in 2-month-old sciatic nerves and it was not upregulated in *L-pgds*$^{-/-}$ nerves (**Supplementary Fig. 3a**). Furthermore, morphological analyses of 1-month-old and 6-month-old *H-pgds*$^{-/-}$ sciatic nerves revealed that, at both ages, *H-pgds*$^{-/-}$ sciatic nerves were normally myelinated (**Supplementary Table 2** and **Supplementary Fig. 3b–g**).

H-pgds$^{-/-}$; *L-pgds*$^{-/-}$ mice are hypomyelinated and myelin is aberrant

To determine whether a lack of both *H-pgds* and *L-pgds* would worsen the hypomyelinating phenotype, we analyzed *in vitro* and *in vivo* myelination in the absence of both enzymes. We first analyzed

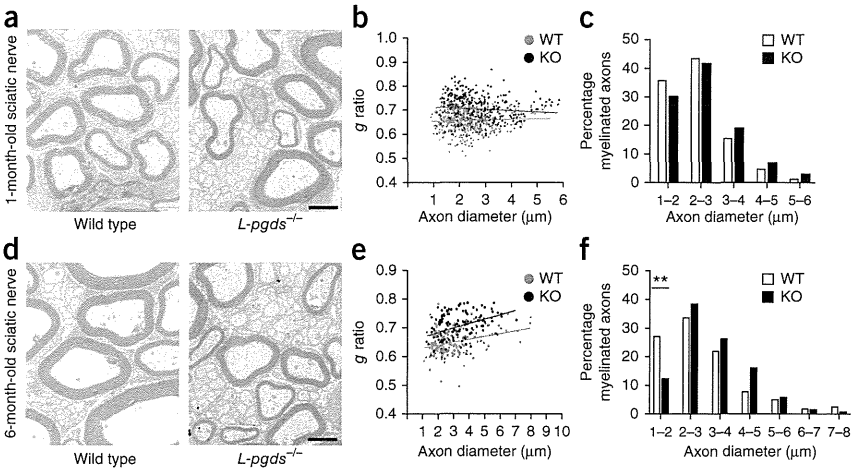

Figure 4 *L-pgds*$^{-/-}$ are hypomyelinated. (**a**–**c**) Morphological analyses of 1-month-old wild-type (WT) and *L-pgds*$^{-/-}$ (KO) sciatic nerves. Electron micrographs (**a**) and *g* ratio analyses (**b**) confirmed hypomyelination in *L-pgds*$^{-/-}$ nerves. *g* ratio was significantly different between wild-type (red line) and *L-pgds*$^{-/-}$ 1-month-old mice (black line; *t* test analysis, $P \leq 0.0001$, $t = 13.19$, df = 782). The graph represents the *g* ratio obtained from more than 300 myelinated axons. (**c**) Distribution of myelinated fibers is similar in *L-pgds*$^{-/-}$ and wild-type 1-month-old sciatic nerves (Fisher's exact test; $P = 0.2811$ (total versus 1–2 μm), $P = 0.7437$ (total versus 2–3 μm), $P = 0.2618$ (total versus 3–4 μm), $P = 0.2776$ (total versus 4–5 μm), $P = 0.1917$ (total versus 5–6 μm)). Over 100 fibers for each genotype were counted. Scale bar represents 2 μm. (**d**–**f**) Morphological analyses of 6-month-old wild-type and *L-pgds*$^{-/-}$ sciatic nerves. Electron micrographs (**d**) and *g* ratio analyses (**e**) confirmed hypomyelination in *L-pgds*$^{-/-}$ nerves. *g* ratio was significantly different between wild-type (red line) and *L-pgds*$^{-/-}$ 6-month-old mice (black line; *t* test analysis, $P \leq 0.0001$, $t = 9.983$, df = 292). The graph represents the *g* ratio obtained from more than 150 myelinated axons. (**f**) Distribution of myelinated fibers is similar in *L-pgds*$^{-/-}$ and wild-type 6-month-old sciatic nerves, with a significant slight decrease in small fibers (1–2 um) in *L-pgds*$^{-/-}$ nerves (Fisher's exact test; $^{**}P = 0.0097$ (total versus 1–2 μm), $P = 0.6492$ (total versus 2–3 μm), $P = 0.595$ (total versus 3–4 μm), $P = 0.0694$ (total versus 4–5 μm), $P = 1$ (total versus 5–6 μm), $P = 1$ (total versus 6–7 μm), $P = 0.3759$ (total versus 7–8 μm)). Over 60 fibers for each genotype were counted. Scale bar represents 2 μm. $N = 3$ mice per genotype at each time developmental time point.

ultrastructural myelin *in vitro* in myelinating co-cultures. We prepared DRG neurons from *H-pgds*$^{-/-}$; *L-pgds*$^{-/-}$ mice at embryonic day 14.5 (E14.5), purified of endogenous Schwann cells and fibroblasts by antimitotic treatment and seeded with wild-type rat Schwann cells. Myelination was induced by adding 50 μg ml^{-1} ascorbic acid for 9 d, after which cultures were processed for immunofluorescence (data not shown) and electron microscopy analyses (**Supplementary Fig. 4**). The number of naked axons was increased in null co-cultures. Notably, *H-pgds*$^{-/-}$; *L-pgds*$^{-/-}$ DRG neurons were substantially hypomyelinated, unlike wild-type controls (**Supplementary Fig. 4c**). Furthermore, we found that, when formed, myelin in *H-pgds*$^{-/-}$; *L-pgds*$^{-/-}$ cultures was aberrant.

Next, we analyzed sciatic nerve morphology in newborn and adult *H-pgds*$^{-/-}$; *L-pgds*$^{-/-}$. We did not observe axonal sorting defects 2 d after birth in *H-pgds*$^{-/-}$; *L-pgds*$^{-/-}$ as compared with controls, although *H-pgds*$^{-/-}$; *L-pgds*$^{-/-}$ fibers were hypomyelinated (**Supplementary Fig. 5a**). We then determined sciatic nerve morphology by electron microscopy analyses and *g* ratio measurements in 7-d-old (**Fig. 5a–c**), 1-month-old (**Fig. 5d–f**) and 9-month-old *H-pgds*$^{-/-}$; *L-pgds*$^{-/-}$ mice (**Fig. 5g–i**). At all ages, *H-pgds*$^{-/-}$; *L-pgds*$^{-/-}$ sciatic nerves fibers were hypomyelinated when compared with those of comparable size in wild-type mice. Morphometric analyses confirmed increased *g* ratio in *H-pgds*$^{-/-}$; *L-pgds*$^{-/-}$ mice versus wild-type littermates (**Supplementary Table 2**), whereas axon diameters in adult nerves were comparable. In addition, in aged *H-pgds*$^{-/-}$; *L-pgds*$^{-/-}$ sciatic nerves, myelin was aberrant (**Fig. 5j,k**), resembling the phenotype observed *in vitro*. We found similar alterations in 6-month-old sciatic nerves of *L-pgds*$^{-/-}$ mice, although the difference was not significant ($P = 0.0649$; **Supplementary Table 2**). Notably, we did not find such alterations in 1-month-old *H-pgds*$^{-/-}$; *L-pgds*$^{-/-}$ nerves, suggesting that these defects are possibly the result of demyelinating events.

To determine whether the hypomyelinating phenotype is more pronounced in sensory nerves, we analyzed myelination in 8-month-old *H-pgds*$^{-/-}$; *L-pgds*$^{-/-}$ saphenous nerves (**Supplementary Fig. 5b–d** and **Supplementary Table 2**). We found that *H-pgds*$^{-/-}$; *L-pgds*$^{-/-}$ nerves were hypomyelinated as compared with wild-type controls. Notably, the total number of myelinated fibers was similar in wild-type and *H-pgds*$^{-/-}$; *L-pgds*$^{-/-}$ motor and sensory roots (**Supplementary Fig. 6a–d**) and distally in sciatic nerves (**Supplementary Fig. 6e**), indicating that *L-pgds* has no effects on neuronal cell number. Similarly, the distribution of axons per Remak bundle was comparable in wild-type and *H-pgds*$^{-/-}$; *L-pgds*$^{-/-}$ nerves at both 1 and 9 months of age (**Supplementary Fig. 6f,g**). Collectively, these findings indicate that L-PGDS is relevant for myelin formation, whereas H-PGDS is dispensable. Furthermore, they suggest that NRG1 backward signaling and PGD2 production are most likely involved in myelin maintenance.

L-PGDS enzymatic activity is important for PNS myelination

Our results suggest that released L-PGDS is enzymatically active. To better investigate its mechanism of action, we inhibited L-PGDS in a Schwann cell–neuronal myelinating co-culture system. We used the specific competitive L-PGDS inhibitor AT-56. To obtain optimal inhibition and avoid toxic effects, we first titrated the amount of AT-56 and compared it with vehicle (DMSO)-treated cultures. We treated isolated rat primary Schwann cells and purified mouse DRG neurons with various AT-56 concentrations for 13 d and monitored cell death by active caspase 3 staining. We found that 50 μM AT-56 induced significant cell death in both neurons (data not shown) and Schwann cells ($P < 0.0001$; **Supplementary Fig. 7a**), whereas 20 and 30 μM AT-56 were well tolerated and did not induce any cell sufferance or death. We analyzed whether 7 d of treatment with 25 and 50 μM AT-56 affected survival in non-myelinating Schwann cell–DRG neuronal co-cultures. We could not detect any caspase 3 activation (**Supplementary Fig. 7c**). Similarly, we did not observe any effect of AT-56 on axon–Schwann cell association (**Supplementary Fig. 7d**).

Next, we induced myelination in organotypic Schwann cell–DRG neuronal co-cultures by adding 50 μg ml^{-1} of ascorbic acid in the presence or absence of AT-56. We added 25 μM AT-56 to the culture media every other day, starting the day before addition of ascorbic acid and continued for 7 or 21 d (**Fig. 6a–d**). Immunofluorescence (**Fig. 6a**)

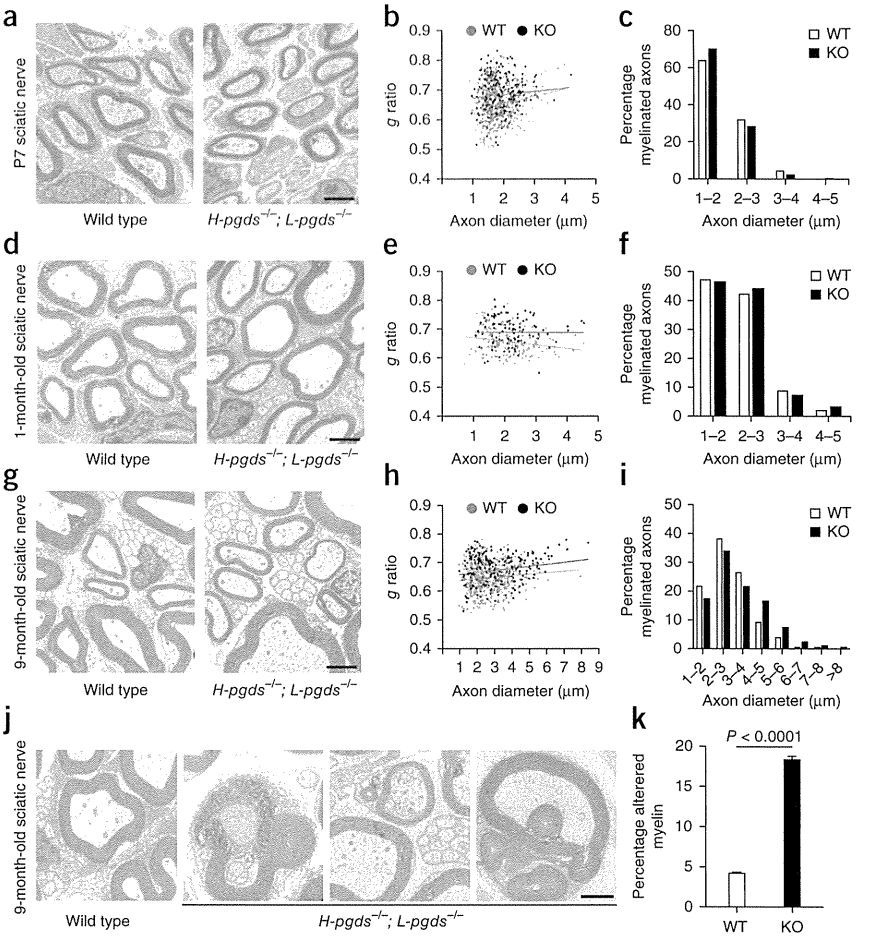

Figure 5 *H-pgds* and *L-pgds* are required for myelin formation and maintenance. (**a–c**) Morphological analyses of P7 wild-type and *H-pgds*$^{-/-}$; *L-pgds*$^{-/-}$ sciatic nerves. Electron micrographs (**a**) and *g* ratio analyses (**b**) confirmed hypomyelination in *H-pgds*$^{-/-}$; *L-pgds*$^{-/-}$ nerves. *g* ratio was significantly different between wild-type (red line) and P7 *H-pgds*$^{-/-}$; *L-PGDS*$^{-/-}$ (black line; *t* test analysis, $P \leq 0.0001$, $t = 6.308$, df = 713). The graph represents the *g* ratio obtained from more than 300 myelinated axons. (**c**) Distribution of myelinated fibers was similar in *H-pgds*$^{-/-}$; *L-pgds*$^{-/-}$ and wild-type P7 sciatic nerves (Fisher's exact test; $P = 0.4774$ (total versus 1–2 μm), $P = 0.5307$ (total versus 2–3 μm), $P = 0.0808$ (total versus 3–4 μm), $P = 1$ (total versus 4–5 μm)). Over 100 fibers for each genotype were counted. $N = 3$ mice per genotype. Scale bar represents 2 μm. (**d–f**) Morphological analyses of 1-month-old wild-type and *H-pgds*$^{-/-}$; *L-pgds*$^{-/-}$ sciatic nerves. Electron micrographs (**d**) and *g* ratio analyses (**e**) confirmed hypomyelination in *H-pgds*$^{-/-}$; *L-pgds*$^{-/-}$ nerves. *g* ratio was significantly different between wild-type (red line) and *H-pgds*$^{-/-}$; *L-pgds*$^{-/-}$ (black line; *t* test analysis, $P \leq 0.0001$, $t = 6.104$, df = 272). The graph represents the *g* ratio obtained from more than 120 myelinated axons. (**f**) Distribution of myelinated fibers is similar in *H-pgds*$^{-/-}$; *L-pgds*$^{-/-}$ and wild-type 1-month-old sciatic nerves (Fisher's exact test; $P = 0.9143$ (total versus 1–2 μm), $P = 0.9124$ (total versus 2–3 μm), $P = 0.8245$ (total versus 3–4 μm), $P = 0.7071$ (total versus 4–5 μm)). Over 40 fibers for each genotype were counted. $N = 3$ mice per genotype. Scale bar represents 2 μm. (**g–i**) Morphological analyses of 9-month-old wild-type and *H-pgds*$^{-/-}$; *L-pgds*$^{-/-}$ sciatic nerves. Electron micrographs (**g**) and *g* ratio analyses (**h**) confirmed hypomyelination in *H-pgds*$^{-/-}$; *L-pgds*$^{-/-}$ nerves. *g* ratio was significantly different between wild-type (red line) and *H-pgds*$^{-/-}$; *L-pgds*$^{-/-}$ (black line; *t* test analysis, $P \leq 0.0001$, $t = 6.386$, df = 694). The graph represents the *g* ratio obtained from more than 300 myelinated axons. (**i**) Distribution of myelinated fibers is similar in *H-pgds*$^{-/-}$; *L-pgds*$^{-/-}$ and wild-type 9-month-old sciatic nerves (Fisher's exact test; $P = 0.6116$ (total versus 1–2 μm), $P = 0.5183$ (total versus 2–3 μm), $P = 0.5299$ (total versus 3–4 μm), $P = 0.0754$ (total versus 4–5 μm), $P = 0.162$ (total versus 5–6 μm), $P = 0.2168$ (total versus 6–7 μm), $P = 1$ (total versus 7–8 μm), $P = 1$ (total versus >8 μm)). Over 100 fibers for each genotype were counted. $N = 3$ mice per genotype. Scale bar represents 2 μm. (**j**) Electron microscopy images of 9-month-old myelinated fibers in wild-type and *H-pgds*$^{-/-}$; *L-pgds*$^{-/-}$ sciatic nerves. Myelin was aberrant in *H-pgds*$^{-/-}$; *L-pgds*$^{-/-}$, but not in wild-type, fibers. $N = 3$ mice per genotype. Scale bar represents 2 μm. (**k**) Graph representing the percentage of axons with altered myelination in *H-pgds*$^{-/-}$; *L-pgds*$^{-/-}$ versus wild-type 9-month-old mice. All counting was performed on reconstructed sciatic nerve and the results expressed relative to the total number of myelinated fibers. Over 1,000 fibers for each genotype were counted (*t* test analysis, $P \leq 0.0001$, $t = 24.17$, df = 4). $N = 3$ mice per genotype. Error bars represent mean ± s.e.m.

and western blot analyses (**Fig. 6b**) revealed that AT-56 addition substantially inhibited myelin basic protein (MBP) and myelin protein zero (MPZ) expression as compared with untreated or DMSO-treated cultures with a dose-dependent effect (**Supplementary Fig. 7b**), but had no effect on internodal length (**Fig. 6d**). We further confirmed these results by assessing the numbers of MBP$^+$ segments, which were significantly diminished in AT-56 treated as compared with untreated or DMSO-treated co-cultures ($P < 0.0001$; **Fig. 6c**). These data confirm that L-PGDS enzymatic activity is important in myelin formation, although we cannot exclude the possibility that AT-56 might affect Schwann cells survival and/or axon association in myelinating conditions.

Our *in vivo* analyses suggest that PGD2 might be important for myelin maintenance. Thus, we inhibited L-PGDS signaling *in vitro* in already myelinated cultures. We added 25 μM AT56 to wild-type Schwann cell neuronal co-cultures that had already been myelinated for 21 d. Cultures were maintained for an additional 7 d and the inhibitor was added every other day (concomitantly with the change of media). AT-56 treatment resulted in marked demyelination (**Fig. 6e**), as corroborated also electron microscopy analyses (**Fig. 6f**). These results confirm that NRG1 backward signaling and PGD2 production might be involved in myelin maintenance.

Gpr44 regulates PNS myelination

PGD2 can bind to two G protein–coupled transmembrane receptors: *Gpr44* (also known as *Ptgdr2* or *Crth2*) and *Ptgdr* (also known as *DP*). To determine which receptor is the target of PGD2, we investigated mRNA expression levels of both receptors by quantitative PCR (qPCR) in DRG neurons that were either infected or not with NRG1 ICD and in purified primary rat Schwann cells. Although *Ptgdr* expression level was similar in all samples (**Supplementary Fig. 8a**), *Gpr44* was highly expressed in purified primary rat Schwann cells as compared

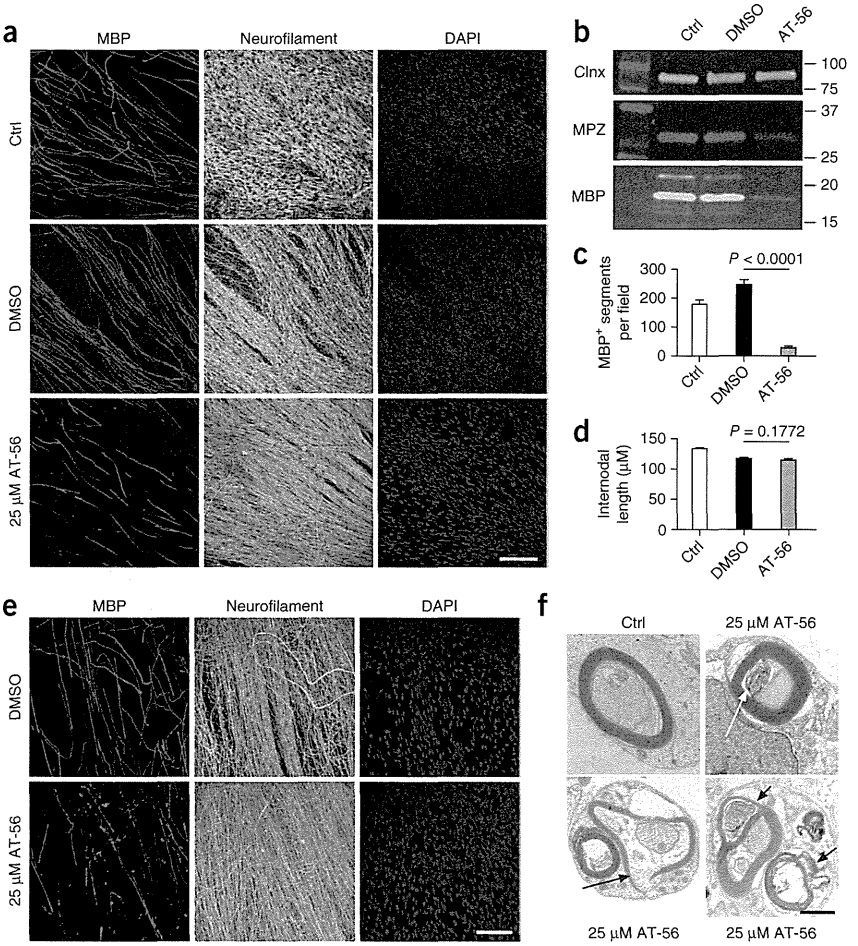

Figure 6 L-PGDS enzymatic activity is important for PNS myelination and maintenance. (**a**) Representative immunofluorescence of co-cultures of organotypic rat Schwann cells and DRG neurons treated with 25 μM AT-56 for 7 d in the presence of ascorbic acid to induce myelination. AT-56 treatment was started the day before ascorbic acid addition and the compound was added every other day. After 7 d in myelinating conditions, cultures were fixed and stained for MBP (rhodamine), neurofilament (fluorescein) and nuclei (DAPI, blue). AT-56 treatment substantially impaired myelination. $N = 5$ different independent co-culture experiments. Scale bar represents 100 μm. (**b**) Representative western blotting analyses of organotypic rat Schwann cell–DRG neuronal co-cultures treated with 25 μM AT-56 for 21 d in myelinating conditions. Lysates were tested for MPZ, MBP and calnexin (Clnx) as a loading control. MBP and MPZ expression were substantially reduced in the presence of AT-56. For uncropped pictures of western blots, see **Supplementary Figure 10**. $N = 5$ different independent experiments. (**c**) Average of three different experiments showing quantitation of MBP$^+$ segments 7 d after induction of myelination in control and 25 μM AT-56–treated co-cultures. Quantitation was performed on the entire culture (t test analyses, $P \leq 0.0001$, $t = 13.66$, df = 76 DMSO – AT-56). Error bars represent mean ± s.e.m. $N = 39$ cultures per condition from three different independent experiments. (**d**) Representative graph showing internodal length of 216 MBP$^+$ segments per condition 21 d after induction of myelination in control and 25 μM AT-56–treated co-cultures. The distance between Nodes of Ranvier was determined by co-staining myelinated cultures with the paranodal marker Caspr. AT-56 treatment had no effect on internodal length (t test analyses, $P = 0.1772$, AT-56–DMSO $t = 1.352$, df = 430). Error bars represent mean ± s.e.m. $N = 216$ segments per condition from three different independent experiments. (**e**) Representative immunofluorescence of already myelinated organotypic rat Schwann cell–DRG neuronal co-cultures (21 d of ascorbic acid) were treated with 25 μM AT-56 for an additional 7 d in myelinating conditions. At the end of the treatment, cultures were fixed and stained for MBP (rhodamine), neurofilament (fluorescein) and nuclei (DAPI, blue). AT-56 treatment in already myelinated cultures induced myelin degeneration. $N = 3$ different independent co-culture experiments. Scale bar represents 100 μm. (**f**) Representative electron microscopy analyses of untreated or 25 μM AT-56–treated Schwann cell–DRG neuronal co-cultures. As in **e**, cultures were allowed to myelinate for 21 d, then treated with 25 μM AT-56 or DMSO as control for additional 7 d. Signs of myelin damage (arrows) were observed only in AT-56–treated cultures resembling those observed *in vivo*. $N = 9$ different independent co-culture experiments. Scale bar represents 1 μm.

with DRG neurons, either infected or not (**Fig. 7a**), suggesting that Gpr44 might function as a glial receptor for PGD2.

Thus, we inactivated *Gpr44* expression using shRNA lentiviral-mediated knockdown *in vitro*. We used three different shRNA clones (shA3, shA5 and shC9) obtained from the siRNA Consortium together with a lentiviral vector expressing a scrambled artificial sequence as a negative control[4]. BLAST analyses confirmed that the targeted sequences, although originally designed in mouse, also recognized rat *Gpr44*. We corroborated efficient knockdown in infected rat primary Schwann cells by qPCR analyses. Two of three *Gpr44* shRNA significantly ablated the expression of *Gpr44* (50–70% reduction; shA3, $P \leq 0.001$; shC9, $P \leq 0.0001$; **Fig. 7b**) when compared with that of not infected or scramble-infected cultures.

We then infected mouse DRG explant cultures containing both Schwann cells and neurons with *Gpr44* shRNA or scramble shRNA as described previously[4]. Cultures were grown without antimitotic agents to allow infection of both neurons and Schwann cells. Myelination was induced by supplementing the cultures with 50 μg ml^{-1} ascorbic acid for 7 d, after which they were analyzed by immunohistochemistry for MBP and neurofilament expression (**Supplementary Fig. 8b**). Notably, downregulation of Gpr44 impaired the extent of myelination *in vitro* in organotypic myelinating co-cultures.

To determine the cell autonomous role of Gpr44, we knocked down its expression in isolated primary rat Schwann cells and co-cultured them with purified mouse wild-type neurons. Efficient knocked down was determined on isolated Schwann cells by qRT-PCR analyses before seeding onto neurons using primers specific for *Gpr44* (**Fig. 7b**). Cultures were maintained in myelinating conditions for 21 d. Immunofluorescence (**Fig. 7c**) and western blotting (**Fig. 7d**) analyses for MBP and neurofilament revealed that ablation of glial Gpr44 substantially impaired myelination, suggesting that *Gpr44* acts Schwann cell autonomously *in vitro*.

To further validate Gpr44's role in PNS myelination, we analyzed *in vivo* myelination in 2-month-old *Gpr44*$^{-/-}$ sciatic nerves. Electron microscopy analyses showed that these nerves were hypomyelinated (**Fig. 7e**). Morphometric analyses confirmed an increased g ratio in

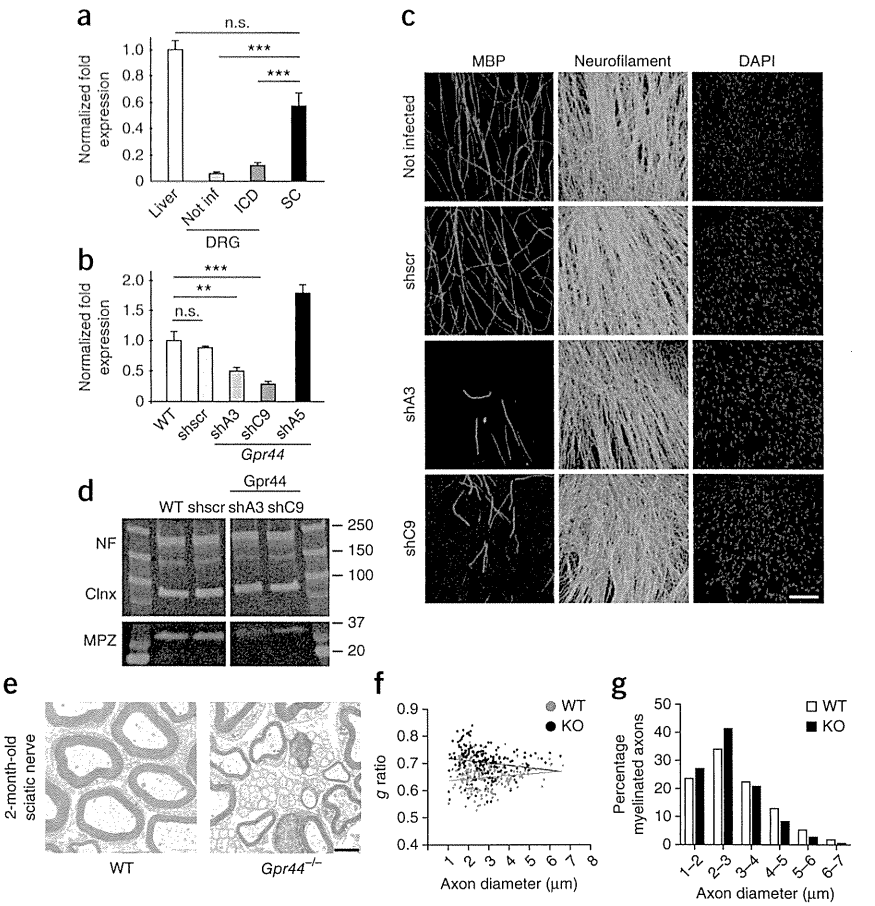

Figure 7 Gpr44 promotes myelination. (**a**) *Gpr44* qRT-PCR analyses in mRNA prepared from not infected or NRG1 ICD–infected DRG neurons, primary rat Schwann cells and liver, which serves as a control. *Gpr44* was significantly expressed in primary rat Schwann cells. Expression levels were normalized to *Gapdh* levels. Data were analyzed with the CFX Manager Software on three mRNA different preparations. Error bars represent mean ± s.d. (one-way ANOVA, $F = 114$, $^{***}P \leq 0.0001$ SC – not inf, $^{***}P \leq 0.0001$ SC – ICD, $P = 0.1755$ SC – liver). $N = 3$ different independent mRNA preparations and analyses. n.s. indicates not significant ($P = 0.1755$). (**b**) Average of three different experiments showing approximately 70% reduction in *Gpr44* expression in Schwann cells infected with *Gpr44* shRNAs (shA3, shC9). Expression levels were determined by qRT-PCR analyses in mRNA prepared from *Gpr44* shRNA–infected, not infected or scramble-infected Schwann cells, which serve as control, and normalized to *Gapdh* levels. Data were analyzed with the CFX Manager Software on three mRNA different preparations. Error bars represent means ± s.e.m. (one-way ANOVA, $F = 98.33$, $^{**}P \leq 0.001$ wild type – shA3, $^{***}P \leq 0.0001$ wild-type – shC9, $P = 0.6408$ wild type – shscr). $N = 3$ different independent infections performed with three different vital stock preparations. (**c**) Representative immunofluorescence of co-cultures of uninfected wild-type mouse DRG neurons purified of endogenous Schwann cells and repopulated with rat Schwann cells previously infected with *Gpr44* shRNA (shA3 or shC9) or scrambled shRNA (shscr). Cultures were maintained in myelinating conditions for 21 d, then stained for MBP (rhodamine) and neurofilament (fluorescein). Fewer myelin segments were evident in shA3- and shC9-treated cultures. $N = 3$ different independent co-culture experiments. Scale bar represents 100 μm. (**d**) Representative western blotting analyses of wild-type uninfected mouse DRG neurons purified of endogenous Schwann cells and repopulated with rat Schwann cells previously infected with shA3, shC9 or shscr. Lysates were tested for MPZ, neurofilament (NF) and calnexin as a loading control, 14 d after induction of myelination. MPZ expression was substantially reduced in *Gpr44* knocked down cultures. For uncropped pictures of western blots, see **Supplementary Figure 10**. $N = 3$ different independent experiments. (**e–g**) Morphological analyses of 2-month-old wild-type and $Gpr44^{-/-}$ sciatic nerves. Electron micrographs (**e**) and *g* ratio analyses (**f**) confirmed hypomyelination in $Gpr44^{-/-}$ nerves. *g* ratio was significantly different between wild-type (red line) and $Gpr44^{-/-}$ (black line) nerves (*t* test analysis, $P \leq 0.0001$, $t = 8.048$, df = 391). The graph represent the *g* ratio obtained from more than 150 myelinated axons. (**g**) Distribution of myelinated fibers was similar in $Gpr44^{-/-}$ and wild-type 2-month-old sciatic nerves (Fisher's exact test; $P = 0.5733$ (total versus 1–2 μm), $P = 0.3816$ (total versus 2–3 μm), $P = 0.8086$ (total versus 3–4 μm), $P = 0.182$ (total versus 4–5 μm), $P = 0.2889$ (total versus 5–6 μm), $P = 0.3219$ (total versus 6–7 μm)). Over 70 fibers for each genotype were counted. $N = 3$ mice per genotype. Over 60 fibers for each genotype were counted. Scale bar represents 2 μm.

$Gpr44^{-/-}$ mice versus wild-type littermates (**Supplementary Table 2**), mainly in small fibers, whereas axon diameters in adult nerves were comparable (**Fig. 7f,g**). Collectively, these results indicate that Gpr44 participates in PNS myelination, although we could not prove that it is directly activated by L-PGDS, as the addition of 15R-methyl-prostaglandin D2, a specific Gpr44 agonist, had a toxic effect onto $H\text{-}pgds^{-/-}$; $L\text{-}pgds^{-/-}$ *in vitro* co-cultures (data not shown).

PGD2 activates Nfatc4 in Schwann cells

We sought to determine the signaling pathways activated by PGD2 in Schwann cells. Previous studies in immune cells reported that Gpr44 activation can mobilize intracellular Ca^{2+} storage or modulate intracellular levels of cAMP[16]. Notably, in PNS myelination, PLC-γ, via the NRG1/erbB pathway, increases intracellular Ca^{2+} levels and promotes nuclear translocation of the transcription factor Nfatc3/c4 in Schwann cells to induce myelination[18]. Furthermore, elevation of cAMP in rat primary Schwann cells activates transcription of myelin genes[29,30]. In addition to these pathways, NRG1 type III specifically activates the PI-3 kinase pathway[31,32], and recent studies have shown that ablation of the ERK/MAPK pathways prevents PNS myelination[33].

Thus, we investigated which signaling pathways, among those implicated in myelination, are activated by PGD2. Primary rat Schwann cells were grown to confluence, starved for 16 h, stimulated with 100 nM PGD2 for 30 min at 37 °C, lysed and the extracts were run on a SDS gel for western blot analyses. PKA phosphorylation was not altered following PGD2 stimulation, suggesting that PGD2 does not modulate cAMP activity (**Fig. 8a**). Notably, although phospho-AKT, MAPK (**Supplementary Fig. 9a,b**) and calcineurin B1 (**Fig. 8b**) levels were not differentially regulated, PGD2 caused a shift in Nfatc4 phosphorylation (**Fig. 8c**)[18] without altering its total levels. Next, we determined whether Gpr44 knockdown in Schwann cells would alter Nfatc4 phosphorylation. Western blotting analyses did not reveal any effect, indicating either that Nfatc4 could also be modulated by other

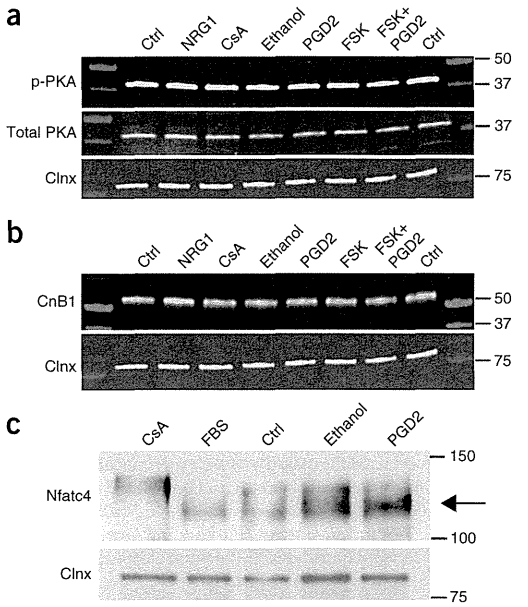

Figure 8 PGD2 induced Nfatc4 dephosphorylation in primary Schwann cells. Rat primary Schwann cells were grown to confluence and then starved for 16 h. Schwann cells were treated with 2.5 ng ml^{-1} NRG1β1, 10 nM cyclosporin A, 100 nM ethanol, 100 nM PGD2, 2.5 μM forskolin, 100 nM PGD2 and 2.5 μM forskolin. (**a**,**b**) Schwann cells lysates were tested by western blotting analyses for phosphorylated and total PKA levels (**a**) and for calcineurin B1 (**b**), whose expression levels did not change. Images are representative of different experiments. For uncropped pictures of western blots, see **Supplementary Figure 10**. $N = 3$ independent experiments. (**c**) Starved Schwann cells as in **a** were stimulated with 10 nM cyclosporin A, 100 nM ethanol and 100 nM PGD2. In all experiments, not starved (FBS) and starved but not stimulated Schwann cells were also tested (Ctrl). Schwann cells lysates were assayed by western blotting analyses for total Nfatc4 levels. PGD2 induced dephosphorylation of Nfatc4 (arrow). Image is representative of different experiments. $N = 5$ independent experiments.

receptors or that the knockdown we obtained in primary Schwann cells (50–70%) might not be sufficient (data not shown). Collectively, these results indicate that NRG1 backward signaling specifically activates L-PGDS neuronal release and most likely activates Gpr44 on Schwann cells, identifying a previously unknown pathway in PNS myelination (**Supplementary Fig. 9c**).

DISCUSSION

Regulated intramembrane proteolysis is a highly conserved mechanism, allowing fast communication from the plasma membrane to the cell nucleus, where the response to extracellular stimuli is normally achieved by activating the transcription of specific genes[34]. Our data indicate that, in the PNS, NRG1 type III, similar to other growth factors, is processed following a regulated intramembrane proteolysis mechanism. Furthermore, our data describe a previously unknown, pharmacologically accessible level of communication between Schwann cells and neurons. We found that Schwann cells are important regulators of NRG1 processing together with the γ-secretase complex. Although our preliminary data show that erbB receptors are not sufficient to mediate NRG1 cleavage (data not shown), it is possible that they act in synergy with other molecules.

Our main result is the identification of L-PGDS and of the G protein–coupled receptor Gpr44, which has almost exclusively been implicated in inflammatory processes[35], as key determinants in PNS myelin formation and maintenance. Collectively, our data suggest that this class of molecules is not simply a key mediator of cell-cell interaction in dendritic cells[36], but exerts this role in other biological systems, including PNS.

We found that, following NRG1 intracellular domain cleavage and nuclear translocation, *L-pgds* mRNA was upregulated inside the neurons, whereas L-PGDS protein was secreted. Although L-PGDS secretion has been reported in other systems[11,20,27,37], how this is achieved in PNS is currently unknown. Previous studies have shown that L-PGDS is released together with PGD2 via exosomes. In addition to L-PGDS and PGD2, exosomes contain all of the enzymes and substrates necessary for prostaglandin production, including arachidonic acid, Cox-1 (Ptgs1), Cox-2 (Ptgs2) and PGH2, suggesting that these vesicles can behave as carriers of bioactive lipids[22]. Whether *L-pgds* mRNA is transported along neurites and then locally translated before insertion in exosomes has not yet been determined. Alternatively, L-PGDS protein, similar to BDNF, could be internally synthesized and immediately processed by fast transport turnover[38]. As in the case of BDNF in fact, L-PGDS endogenous neuronal levels are extremely limited, thus L-PGDS protein might be translated in neurons and then trafficked trough the secretory pathway by chaperone proteins[39].

Previous studies have implicated the NRG1 intracellular domain in the promotion of neuronal survival[5]. Unlike these results, we could not confirm that NRG1 ICD has a similar role *in vitro* in DRG neurons and we could not find alterations in the number of myelinated fibers *in vivo*. Our study differs from the previous one[5] in that we investigated NRG1 ICD in PNS neurons, whereas the previous study used hippocampal neurons, suggesting that the effects of NRG1 ICD could vary in different neuronal populations. It is also possible, however, that *in vitro* analyses of neuronal survival mediated by these prostanoids might be masked[40].

Notably, NRG1 ICD specifically and substantially upregulated the expression of *L-pgds*, which is enzymatically active to produce the bioactive prostaglandin PGD2. We found that PGD2 most likely activated Gpr44 on Schwann cells to promote myelin formation. Stimulation of Gpr44 ultimately led to dephosphorylation of the transcription factor Nfatc4, a triggering event for the expression of *Egr2* and *MPZ*[18]. Consistent with a previous study[18], we also found that activation of Nfatc4 was independent of the PI-3 kinase and MAPK pathways, but was specifically modulated by PGD2. Unlike previous studies, activation of Nfatc4 downstream of PGD2 did not require increased levels of intracellular cAMP[41], although cAMP might cooperate with PGD2 to activate Nfat in Schwann cells.

In our analyses, we also characterized a G protein–coupled receptor, Gpr44, that participated in PNS myelination. The role of G protein–coupled receptors in myelination has been studied previously. Although many have been implicated in the control and modulation of CNS myelination and remyelination[42,43], the only member of this family thus far implicated in PNS myelination is adhesion G protein–coupled receptor 126 (Gpr126), in both zebrafish[44] and mammals[45]. Gpr126 activity, unlike Gpr44, is dependent on PKA phosphorylation[46,47] and increased intracellular levels of cAMP[47]. Recent studies have shown that, at least in zebrafish, the pathways activated by NRG1 type III and Gpr126 are both required for initiation of myelination *in vivo*, but that different signals control initiation and maturation of myelin[46]. Our results suggest that Gpr44 could be part of the signaling machinery that, in synergy with NRG1 type III, could be involved in myelin maintenance. Nonetheless, we cannot exclude the possibility that other PGD2 receptors, particularly Ptgdr, which is expressed by both Schwann cells and neurons, might participate.